THE JOURNAL OF PHYSICAL CHEMISTRY C

Article

pubs.acs.org/JPCC

Graphene Scaffolds Enhanced Photogenerated Electron Transport in ZnO Photoanodes for High-Efficiency Dye-Sensitized Solar Cells

Feng Xu,*[,†] Jing Chen,[‡] Xing Wu,[†] Yi Zhang,[†] Yuxi Wang,[†] Jun Sun,[†] Hengchang Bi,[†] Wei Lei,[‡] Yaru Ni,[§] and Litao Sun*[,†]

[†]SEU-FEI Nano-Pico Center, Key Laboratory of MEMS of Ministry of Education, and [‡]Jiangsu Information Display Engineering Research Center, School of Electronic Science and Engineering, Southeast University, Nanjing 210096, China

[§]State Key Laboratory of Materials-Oriented Chemical Engineering, Nanjing University of Technology, Nanjing 210009, China

Supporting Information

ABSTRACT: Graphene and ZnO as two star materials were united to constitute the photoanode of dye-sensitized solar cells (DSSCs). Highly electronically conductive graphene scaffolds incorporated into ZnO hierarchically structured nanoparticle (HSN) photoanodes could simultaneously capture and transport photogenerated electrons injected into ZnO by excited dyes. This strategy was beneficial for electrons to fluently transfer to the collection electrode due to the decreased internal resistance and electron recombination loss. On the basis of these advantages, the DSSC incorporating 1.2 wt % graphene into the ZnO photoanode with 3 μm in thickness exhibited a high short-circuit photocurrent density (J_{sc}) of 10.89 mA/cm^2 and a power conversion efficiency (PCE) of 3.19%, which were increased by 43.48% and 38.09%, respectively, compared with those of the DSSC without graphene. It was found that the incorporated graphene could markedly prolong electron lifetime (τ_{eff}) and effective diffusion length (L_n), which allowed the utilization of thicker photoanodes that could afford enhanced surface area for higher dye loading and light harvesting. Thus, an impressively high PCE of 5.86% was achieved for the DSSC composed of 9-μm-thick ZnO photoanode, which could be the highest PCE compared with previous reports with the same thick photoanodes. These results demonstrate potential application of graphene for improving the performance of DSSCs.

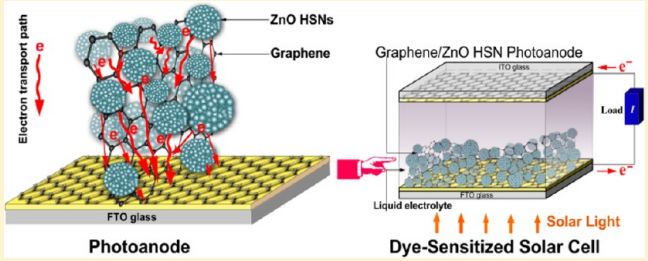

1. INTRODUCTION

As a photovoltaic device, the dye-sensitized solar cell (DSSC) has recently emerged as a cost-effective alternative to conventional silicon photovoltaic devices at a very competitive cost.[1] In ZnO-based DSSCs, ZnO nanoparticle photoanodes with a high surface area have been extensively studied.[2−9] Further enhancement in power conversion efficiency (PCE) by arbitrarily increasing the thickness of the photoanode to obtain higher dye loading and light harvesting has been limited by serious energy loss due to recombination between injected electrons and either the oxidized dye molecules or the electron-accepting species in the electrolyte during the electron transfer process across the ZnO nanoparticle network.[10−12] Therefore, the utilization of 1D[13−18] and 2D[19−21] ZnO nanostructure arrays as the photoanodes is expected to significantly extend the effective electron diffusion length (L_n) by providing a direct conduction pathway for rapid transport of photogenerated electrons to the collection electrode, which would diminish the possibility of electron recombination as in the nanoparticle network. However, the insufficient surface area of these simple 1D and 2D ZnO nanostructure arrays sacrifices the dye loading and hence limits the further increase in PCE. In this regard, composite ZnO nanostructures combining multidimensional and hierarchical configurations (e.g., nanopartilces/nanorod arrays,[22,23] nanowires/nanosheet arrays,[24,25] nanoforest[26]) seem to be desirable due to their increased surface area and reduced electron recombination. Even so, from the viewpoint of the large surface area, facile manufacture, and high PCE, the photoanodes based on ZnO nanoparticles with hierarchical structures are still attractive.[2] Therefore, if we can commendably deal with serious electron recombination in nanoparticulate photoanodes by introducing charge carriers to direct electron transport toward the collection electrode, the improved cell performance with a considerably high PCE could be achieved.[27]

In this work, we incorporated the 2D graphene scaffolds with high electron mobility[28] into ZnO hierarchically structured nanoparticle (HSN) photoanodes to act as charge carriers (as shown in Scheme 1). The interconnected graphene scaffolds serve as the "tentacle" to capture the injected electrons and as the "speedway" to enhance the electron transport rate for suppressing the electron recombination. To the best of our knowledge, there have been no reports on the enhancement of DSSCs by incorporating graphene into the matrix of ZnO photoanodes, other than simple surface modification and acting as collecting electrodes. Moreover, this strategy allows the

Received: December 16, 2012
Revised: March 24, 2013
Published: April 2, 2013

Scheme 1. Schematic Diagram of the Graphene/ZnO HSN Composite Photoanode and Possible Electron Transport Path within the Structure

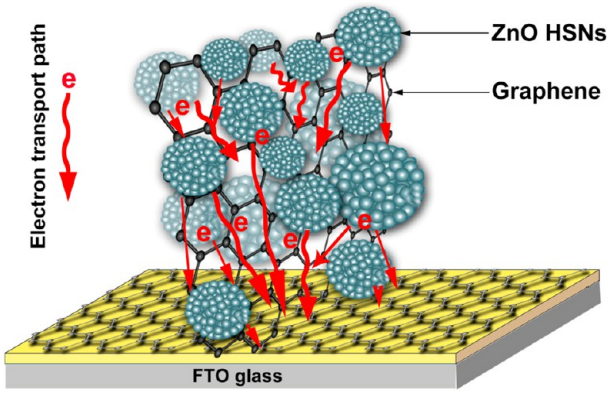

utilization of thicker photoanodes due to longer electron lifetime and longer electron effective diffusion length, resulting in larger surface area for higher dye loading and light harvesting. It was expected that the DSSCs using the graphene/ZnO HSN composite photoanodes with graphene scaffolds could yield an impressively high PCE compared with the ones using the photoanodes with ZnO nanoparticles alone.

2. EXPERIMENTAL SECTION

2.1. Synthesis of Graphene Oxide (Precursor to Graphene) and ZnO HSNs. Graphene oxide (GO) was prepared by chemically exfoliating expandable graphite (EG)[29] based on a modified Hummers method by us.[30] ZnO HSNs were synthesized by the solvothermal process of zinc salt in polyol medium, similar to the method reported by D. Jezequel et al.[31] Detailed synthesis procedures can also be found in Supporting Information.

2.2. Preparation of Graphene/ZnO HSN Composite Photoanode. Graphene/ZnO HSN composite photoanodes were obtained by in situ reducing GO incorporated into ZnO HSN films. To prepare GO/ZnO composite electrodes, 6 g of PVA (MW 22 000) was added to 14 mL of boiled DW with powerful stirring, forming a highly viscous liquid that was further diluted in the mixed solvent (18 mL DW and 25 mL ethanol) at above 70 °C. Then, 1.62 g of as-synthesized ZnO HSNs was added in batches to make the suspension of ZnO. After this, 2.5 mL of GO aqueous solution with a certain concentration (1−10 mg/mL) was added into the suspension that was kept at continuous stirring for 2 h to enable good GO dispersion in the suspension. Subsequently, GO/ZnO composite suspension was cooled to room temperature and used to prepare the photoanode films by the doctor-blade technique on graphene/fluorine-doped tin oxide (FTO, 15 Ω/□) glass substrates, and the photoanode thickness could be modulated by controlling doctor-blade film-preparation times. The graphene/FTO electrode was prepared by a filtration-transfer-reduction method[32] that was initially developed for fabricating transparent, conductive CNT films. The preparation procedure of the graphene/ITO electrode can be schematically described as Scheme S1 in Supporting Information. The as-prepared photoanodes were placed in vacuum at 120 °C for 5 h to evaporate water and ethanol. Afterward, the electrodes were annealed at 450 °C under nitrogen gas flow for 5 h, and the GO was reduced to graphene totally. Lastly, the electrodes were calcined at 500 °C for 3 h. It is worth noting that the temperature increase or decrease must be controlled at very slow rate during the annealing and calcining processes of photoanodes. Pure ZnO HSN photoanodes were also prepared for comparison by doctor-blade technique on the graphene/FTO substrates.

2.3. Assembly and Testing of DSSCs. The fabrication of DSSCs was performed as follows: Dying of the graphene/ZnO composite photoanodes was performed in *cis*-bis-(isothiocyanato)bis(2,2′-bipyridyl-4,4′-dicarboxylato)-ruthenium(II)bis-tetrabutylammonium (N719, Solaronix) dye ethanolic solution (0.3 mM) at 60 °C for 1 h. The photoanodes were then rinsed with ethanol to remove excessive dye molecules that were not directly adsorbed on ZnO and dried in air at room temperature. The sensitized photoanodes were sandwiched together with graphene/ITO counter electrodes separated by hot melt spacers (60 μm thick, Surlyn). The graphene/ITO electrodes were prepared by the same filtration−transfer−reduction method.[32] The internal space of the two electrodes was filled with a liquid electrolyte composed of 0.05 M I_2, 0.5 M LiI, 0.5 M 4-*tert*-butylpyridine, and 0.6 M methylhexylimidazolium iodide in acetonitrile by capillary action. The photocurrent−photovoltage (I−V) characteristics of the cell were measured with a Keithley model 2420 digital source meter and a Newport model 94022A solar simulator system (equipped with a 150 W xenon arc lamp, Oriel) at one sun (AM 1.5G, 100 mW/cm^2), which was calibrated with a Si reference solar cell (Model 91150 V, Oriel). The active cell area was typically ∼0.25 cm^2 (defined by a lightproof black mask). The electrochemical impedance spectroscopy (EIS) measurements were performed using an electrochemical workstation (CHI-660D, Shanghai Chenhua Instruments, China) under illumination of one sun (AM 1.5G, 100 mW/cm^2) in the frequency range of 0.01 Hz to 1000 kHz. The applied bias voltage and ac amplitude were set at open-circuit photovoltage (V_{oc}) of the DSSCs and 10 mV between the counter electrode and the working electrode (photoanode), respectively.

2.4. Characterization. The surface morphology and phase identification of the samples were investigated by a scanning electron microscope (SEM, JSM-5900, JEOL, Japan) operated at an acceleration voltage of 15 kV and a powder X-ray diffractometer (XRD, ARL XTRA, Thermo Electron Co., USA) with Cu Kα_B radiation at a scan speed of 5°/min in the 2θ range between 5° and 55°. The tube voltage and the tube current were 45 kV and 35 mA, respectively. Further structural analysis of the samples was carried out using a Cs-corrected high-resolution transmission electron microscope (HRTEM, Titan 80−300, FEI, U.S.A.) with an information limit of 80 pm operated at an acceleration voltage of 300 kV. The TEM was equipped with a multiscan charge-coupled device (CCD) camera system (Model 894, Gatan, USA) to record the HRTEM images and selected area electron diffraction (SAED) patterns. The amount of dye loading was determined by de-adsorbing the dye within the photoanode with 0.1 M NaOH solution and measuring the optical absorbance of dye solutions with a Shimadzu UV-3101PC spectrophotometer.

3. RESULTS AND DISCUSSION

GO was prepared by chemically exfoliating expandable graphite (EG) based on a modified Hummers method. Figure 1 shows the TEM image of free-standing GO nanosheets. The corrugated and scrolled sheets resemble crumpled silk veil waves, indicating their high flexility. Furthermore, the XRD pattern of GO in Figure 2a has a peak centered at 2θ = 11.7°,

dx.doi.org/10.1021/jp312379b | J. Phys. Chem. C 2013, 117, 8619−8627

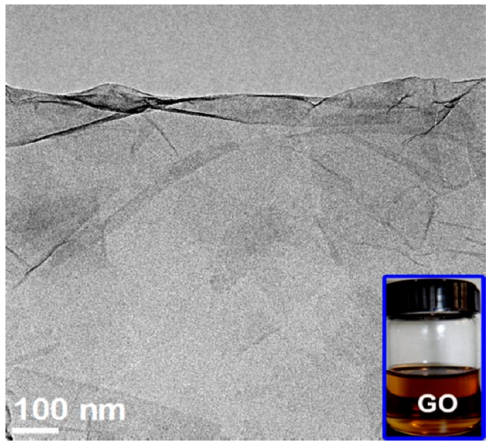

Figure 1. TEM image of as-prepared GO by chemically exfoliating expandable graphite.

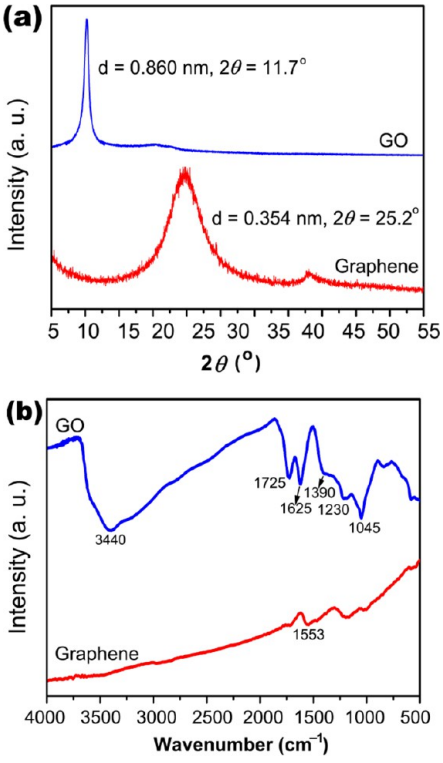

Figure 2. (a) XRD patterns and (b) FT-IR spectra of the pristine GO and the graphene separated from the reduced GO/ZnO HSN composite photoanodes (~1.2 wt % graphene loading).

corresponding to a *d*-spacing of 8.60 Å,[33] which reflects intercalation of oxygen-containing functional groups into the pristine EG. All these confirm that the EG was exfoliated into small GO thin pieces by the strong chemical oxidation process.[34]

GO incorporated into ZnO HSN photoanodes was in situ reduced to graphene by combining chemical reducing and annealing (see Experimental Section 2.2). To corroborate the validity and perfectibility of in situ reduction of GO in the composite photoanodes, the reduced composited photoanodes (~1.2 wt % graphene loading) were first immersed into diluted HCl solution for dissolving ZnO and then the reduced GO that is indissolvable was separated by centrifugation for further characterization. Figure 2a compares the XRD patterns of the pristine GO and reduced GO samples. After reducing GO, the basal spacing decreased from 8.60 Å of the pristine GO to 3.54 Å of the reduced samples, indicating the removal of oxygenated groups and hence the formation of graphene. FT-IR spectra in Figure 2b further validated the conversion from GO to graphene. In FT-IR spectrum of GO, typical vibrations are the strong and broad O−H stretching peak at 3440 cm^{-1}, the C═O stretching peak at 1725 cm^{-1}, the O−H deformation peak at 1390 cm^{-1}, the C−OH stretching peak at 1230 cm^{-1}, and the C−O stretching peak at 1045 cm^{-1}, respectively.[35,36] The peak at around 1625 cm^{-1} due to the O−H bending vibration, epoxide groups, and skeletal ring vibration are also observed, while in the spectrum of graphene, the O−H, C−O, and C═O peaks are almost negligible, and a new peak at around 1553 cm^{-1} appears, which may be attributed to the skeletal vibration of the graphene sheets. All these characterizations imply the feasibility of in situ reduction of GO in the composite photoanodes.

Figure 3 shows a series of SEM images of ZnO HSN photoanode and graphene/ZnO HSN composite photoanode (~1.2 wt % graphene loading), respectively. Surface of ZnO HSN photoanode is porous and the pore size is uniform, as displayed in Figure 3a and c, while incorporating graphene into the ZnO HSN photoanode resulted in more and larger (even in the micrometer scale) pores and obvious surface asperity, as shown in Figure 3b and d. This phenomenon also happened in the case of TiO_2/graphene photoanodes.[37,38] The pores could result from the release of H_2O and N_2H_4 during the reduction and annealing of GO-incorporated ZnO HSN photoanodes. The highly porous graphene/ZnO HSN composite photoanode is expected to have a higher surface area due to the increase in porosity compared with the ZnO HSN photoanode. In addition, one can see from the cross-section SEM images (Figure 3e and f) that both photoanode films possess nearly the same thickness (3 μm), and are tightly adhered to FTO glass substrates. Note that, after reducing GO incorporated into ZnO HSN photoanodes by combining chemical reduction and annealing, the characteristic morphology of polycrystalline ZnO HSNs comprising smaller nanoscale particles was not impaired (see the inset in Figure 3d), which is also consistent with the TEM observation shown in Figure 4a. Further, HRTEM results provide direct evidence of the formation of graphene/ZnO HSN composite structures, and graphene nanosheets have been successfully loaded onto ZnO HSNs (Figure 4b). While on the surface of ZnO HSNs without incorporating graphene, no graphene nanosheets were found, as revealed by Figure 4c.

The DSSC with the graphene/ZnO HSN composite photoanode (~1.2 wt % graphene loading) was assembled, and the configuration of the DSSC resembles the schematic diagram illustrated in Scheme 2. For comparison, the control experiment was also performed using the DSSC constructed by the ZnO HSN photoanode. Figure 5 shows the compared photocurrent−voltage (*J*−*V*) characteristics of both DSSCs under a simulated illumination with a light intensity of 100 mW/cm^2 (AM 1.5). The short-circuit current density (J_{sc}), the open-circuit voltage (V_{oc}), the fill factor (*FF*), the maximum current output (J_{max}), the maximum voltage output (V_{max}), and the power conversion efficiency (PCE) derived from the *J*−*V* curves for both DSSCs are summarized in Table 1. It can be seen from Figure 5 and Table 1 that the J_{sc} (10.89 mA/cm^2) for the DSSC constructed using the graphene/ZnO HSN composite photoanode show an obvious improvement of 43.48% over J_{sc} (7.59 mA/cm^2) of the DSSC constructed using

dx.doi.org/10.1021/jp312379b | J. Phys. Chem. C 2013, 117, 8619−8627

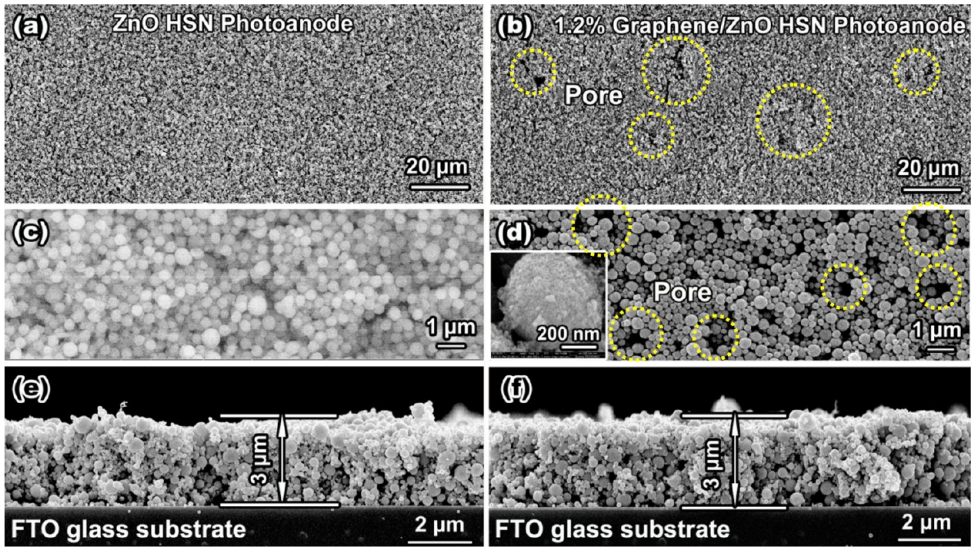

Figure 3. Plan-view SEM images of (a,c) ZnO HSN photoanode and (b,d) graphene/ZnO HSN composite photoanode (~1.2 wt % graphene loading). Inset in panel d is the magnified image of an individual ZnO HSN. (e) and (f) are the cross-section SEM images of ZnO HSN photoanode and graphene/ZnO HSN composite photoanode, respectively.

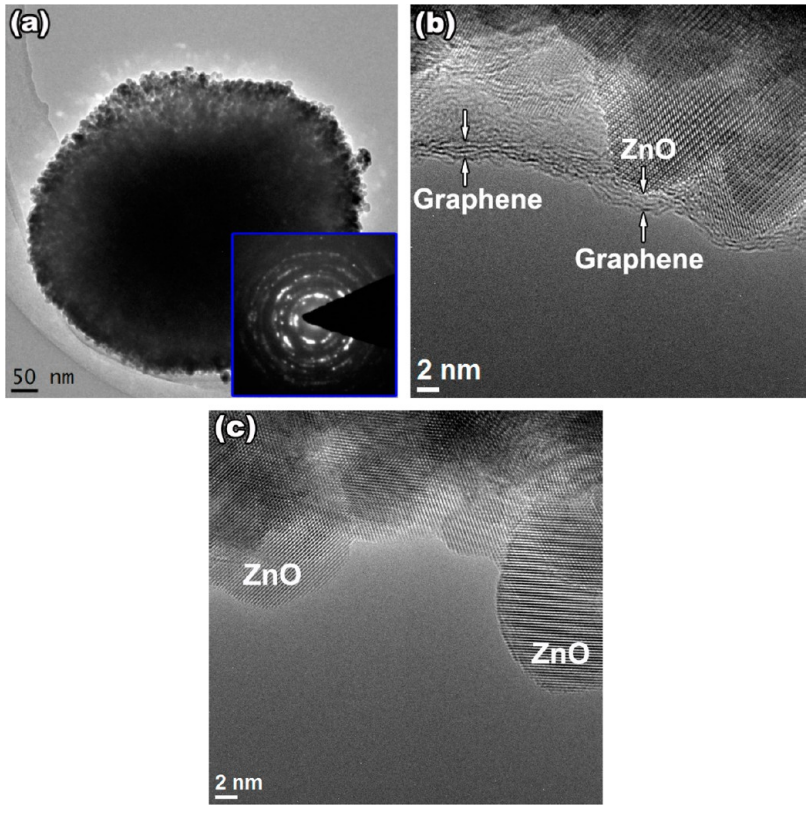

Figure 4. (a) TEM image, SAED pattern, and (b) HRTEM image of an individual ZnO HSN with graphene loading, and (c) HRTEM image of as-prepared ZnO HSN without graphene loading.

the ZnO HSN photoanode. A higher J_{sc} would result in a higher PCE since the PCE is partly dependent on the J_{sc}.[5] Therefore, due to much improved J_{sc}, the graphene/ZnO HSN composite photoanode based DSSC reached a total PCE of 3.19%, which is nearly 38.09% higher than that of the ZnO HSN photoanode based DSSC (2.31%). Besides, the *FF* increased a little from 42.1% to 47.6%. However, there is no great difference in the V_{oc} for both the DSSCs. This phenomenon was also encountered in the case of TiO_2/graphene-based DSSCs.[37,38] However, according to P. V. Kamat's work,[39,40] the incorporation of CNTs into the TiO_2 photoanode resulted in an obvious decrease in the V_{oc} as well as a great increase in the J_{sc}. This was because the apparent Fermi level of CNTs-based photoanode decreased in comparison with that of a pristine photoanode without CNTs, and thus the V_{oc} was sacrificed as a result. Herein, the graphene is a zero band material, and its calculated work function is a little more positive (−4.42 eV vs vacuum) than that of the CNTs. As a result, the apparent Fermi level of

dx.doi.org/10.1021/jp312379b | J. Phys. Chem. C 2013, 117, 8619−8627

Scheme 2. Schematic Diagram of the DSSC Based on the Graphene-Incorporated Hierarchically Structured ZnO Nanoparticale Photoanode

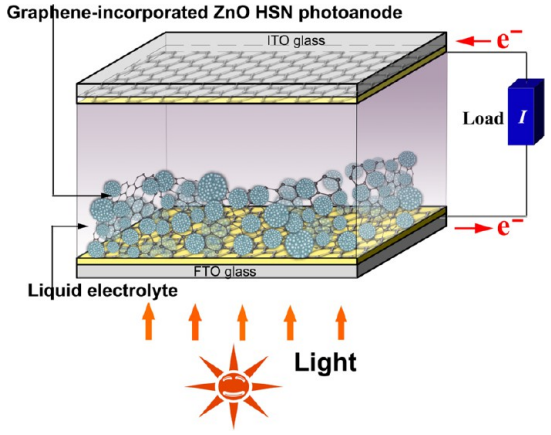

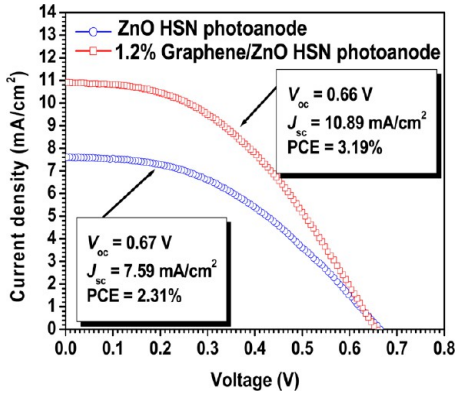

Figure 5. Current−voltage (J−V) characteristics of the DSSCs constructed using the ZnO HSN photoanode and graphene/ZnO HSN composite photoanode (~1.2 wt % graphene loading) under a simulated illumination with a light intensity of 100 mW/cm^2 (AM 1.5).

Table 1. Photovoltaic Parameters of the DSSCs Based on the ZnO HSN Photoanode and Graphene/ZnO HSN (~1.2 wt % Graphene Loading), Respectively

photoanode	thickness (μm)	V_{oc} (V)	J_{sc} (mA/cm^2)	*FF* (%)	PCE (%)
ZnO HSN	3	0.67	7.6	42.10	2.31
Graphene/ZnO HSN (~1.2 wt % graphene loading)	3	0.66	10.89	47.60	3.19

the graphene-based photoanode might not be decreased, and thus the V_{oc} was not affected greatly.

Due to the unconspicuous changes in the V_{oc} and *FF* for both the DSSCs, the increase in J_{sc} should be mainly responsible for the enhancement in the PCE of the DSSC with graphene/ZnO HSN composite photoanode. Generally, the increase in J_{sc} is attributed to several dominant factors including the utilization of photosensitizers with (i) higher extinction coefficient, (ii) the incorporation of photoanodes with larger surface area or functionalized microstructure for more light harvesting, and (iii) the control over recombination of photogenerated electrons. Here, the photosensitizer (N719 dye) adopted is the same for both DSSCs. Moreover, we estimated the amount of dye loading by contrasting the optical absorbance of solutions containing dyes desorbed from the photoanodes (3 μm in thickness) with that of dye solution with a known concentration (see Figure 6). Results show that, for the

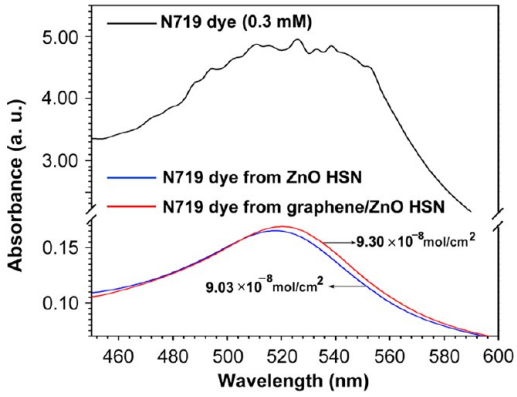

Figure 6. Optical absorbance of solutions containing dyes detached from the ZnO HSN photoanode and graphene/ZnO HSN photoanode, respectively.

graphene/ZnO HSN photoanode, the value is 9.30 × 10^{-8} mol/cm^2 that is increased by 3% in comparison with 9.03 × 10^{-8} mol/cm^2 of ZnO HSN photoanode. Obviously, only 3% increase in dye loading amount is incompatible with the 43.48% increase in the J_{sc}. Thus, the reduced electron recombination should be mainly responsible for the J_{sc} enhancement, which could profit from the incorporation of graphene for rapidly transporting the electrons within the photoanodes.

To corroborate the effect of graphene in transporting the electrons and restraining the back electron transfer, the electrochemical properties of both photoanodes were investigated by electrochemical impedance spectra (EIS) under illumination of one sun (AM 1.5G, 100 mW/cm^2) at an applied bias of V_{oc}, as shown in Figure 7. In the Nyquist plots (Figure 7a), there are two semicircles in high-frequency region and middle-frequency region, respectively. The one in the high-frequency region relates to the charge transfer resistance (R_{ct}) at the electrolyte/counter electrode interface, while the other in the middle frequency region corresponds to the charge transfer resistance (R_w) in the photoanode.[41] The corresponding equivalent circuit of the device is insetted in Figure 7a. Compared with the ZnO HSN photoanode, the semicircle size in the middle frequency for the graphene/ZnO HSN photoanode (1.2 wt % graphene loading) obviously decreases, implying acceleration of the electron transfer process due to lower R_w.[41,42] This result is also supported by the corresponding Bode plots (Figure 7b). The phase shift of the characteristic frequency peak (10−100 Hz) is greatly reduced from 33° for the DSSC with ZnO HSN photoanode to 28° for the DSSC with graphene/ZnO HSN photoanode. Correspondingly, the position of the characteristic frequency peak is shifted to a lower frequency (from 23.5 to 10.7 Hz). Any shift of the peak from high frequency to low frequency reveals a more rapid electron transport process due to longer electron lifetime (τ_{eff}), because the value (f_{mid}) of the middle frequency is related to the inverse of τ_{eff} as follows: $\tau_{eff} = 1/(2\pi f_{mid})$.[42] For the DSSC with the graphene/ZnO HSN composite photoanode, longer electron lifetime (93.4 ms) is obtained compared with 42.5 ms for the DSSC with the ZnO HSN photoanode. Therefore, the Nyquist plots and Bode phase plots show that incorporating graphene into the ZnO HSN photoanode greatly improved the

dx.doi.org/10.1021/jp312379b | J. Phys. Chem. C 2013, 117, 8619−8627

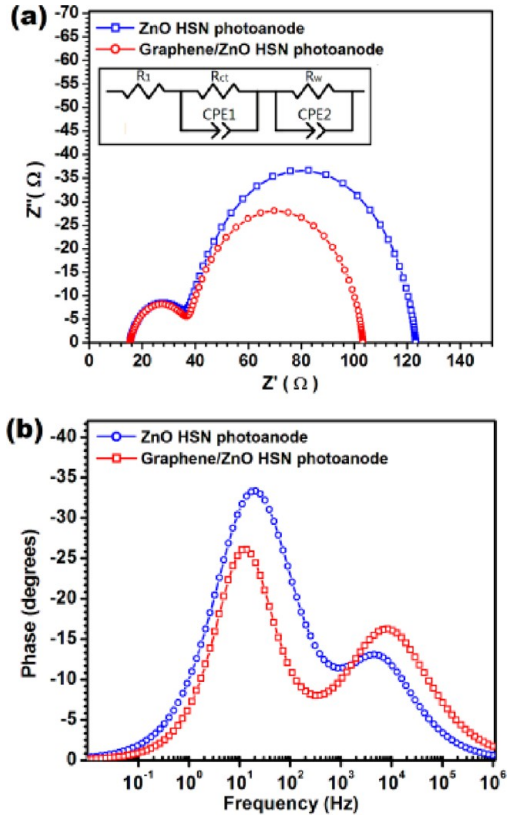

Figure 7. (a) Nyquist and (b) Bode plots of the electrochemical impedance spectra of the ZnO HSN photoanode and graphene/ZnO HSN photoanode. Inset in (a) is the equivalent circuit of the device. The spectra were measured under the illumination of one sun at open-circuit potential.

electrochemical activity due to the prolonged τ_{eff}. In other words, the electrons with longer τ_{eff} can obtain longer effective diffusion length (L_n) and more easily escape the electron recombination. L_n reflects the competition between electron transport and recombination in DSSCs,[43] and it can be derived from the equations, $L_n^2 = D_{eff} \times \tau$ and $D_{eff} = (R_w/R_k)L^2k_{eff}$,[44,45] where R_k, L, and k_{eff} represent the resistance of charge transfer related to the recombination, the thickness of the photoanode, and the effective constant rate for recombination, respectively. These values can be estimated from the central arc of Nyquist and Bode plots according to the suggestion by J. L. Song.[46] The calculated R_w/R_k, k_{eff}, D_{eff}, and the resultant L_n are summarized in Table 2. Obviously, the graphene/ZnO HSN photoanode has a longer L_n (14.43 μm) compared with 8.37 μm of the ZnO HSN photoanode, implying that the former has lower electron recombination.

According to the above-mentioned discussions, we conclude that the incorporation of graphene into the ZnO HSN photoanode can enable the DSSC devices operate more efficiently. Scheme 3 shows the schematic energy diagram of operation principle of the DSSCs with the ZnO HSN photoanode and graphene/ZnO HSN photoanode, respectively. In the photoanode of the latter, as graphene has a work function (−4.42 eV vs vacuum) similar to that of FTO (−4.4 eV vs vacuum),[47] it acts more like many extended "tentacle" penetrating into ZnO HSN matrix for rapidly capturing, transporting, and collecting electrons injected into ZnO before being recombined, and hence the adverse electron transfers (recombination and back transfer) are suppressed in a way, while in the photoanode of the former, photogenerated electrons have to transfer through the ZnO HSN film which is several or even dozens of micrometers thick before reaching the FTO collection electrode. Therefore, the recombination chance for electrons and holes is inevitably increased.

Since the incorporation of graphene into the ZnO HSN photoanode can enhance the PCE of the DSSCs, the graphene loading content should be a paramount factor that directly decides the cell performance. The current−voltage (J−V) characteristics and photovoltaic parameters of the DSSCs based on the graphene/ZnO HSN composite photoanodes with different graphene loading contents are displayed in Figure 8 and Table 3. The results show that the cell PCE would not be enhanced at all times with the increase of graphene loading content, and 1.2 wt % graphene loading is optimal for the 3-μm-thick photoanode. The superfluous graphene increased the probability of contact with the electrolyte and became a kind of recombination center instead of providing an electron pathway.[37] At the same time, the incorporation of excessive graphene led to the cracks of photoanodes that resulted from the excess release of H_2O and N_2H_4 during the reduction of GO. All of these make the short circuit happen easily, causing the decrease of the cell PCE. For instance, the DSSC with even 4.0 wt % graphene loading cannot work at all due to the serious cracks of the photoanodes (see Supporting Information Figure S1).

Based on the EIS analysis, the incorporation of graphene into ZnO HSN photoanodes can prolong the photogenerated electron lifetime (τ) and hence obtain longer effective diffusion length (L_n) and more easily escape from the recombination. This strategy accommodates the utilization of thick photoanodes that could afford enhanced surface area for higher dye loading and light harvesting. Figure 9 and Table 4 show the current−voltage (J−V) characteristics and photovoltaic parameters of the DSSCs based on the graphene/ZnO HSN composite photoanodes with different photoanode thicknesses. With increasing the photoanode thickness from 3 to 9 μm, the short-circuit current density correspondingly rose. Apparently, the PCE also exhibited the similar change trend. The highest PCE of 5.86% was obtained for the DSSC composed of 9-μm-thick graphene/ZnO HSN composite photoanode with 1.2 wt % graphene loading. This value could be the highest among the previous ZnO HSN-based DSSCs with the parallel photoanode thickness,[48,49] as listed in Table 5. Further increasing the photoanode thickness to 25 μm, the short-circuit current density descended promptly. This phenomenon indicates that the prolonged electron lifetime and effective diffusion length

Table 2. Parameters Derived from Nyquist and Bode plots of EIS of the ZnO HSN Photoanode and Graphene/ZnO HSN Photoanode

photoanode	R_w (Ω)	R_k/R_w	k_{eff} (s^{-1})	τ (ms)	τ_{eff} (ms)	D_{eff} (cm^2 s^{-1})	L_n (μm)
ZnO HSN	86	7.8	23.5	42.5	6.8	1.65×10^{-5}	8.37
Graphene/ZnO HSN (~1.2 wt % graphene loading)	65	23.2	10.7	93.4	14.9	2.23×10^{-5}	14.43

dx.doi.org/10.1021/jp312379b | J. Phys. Chem. C 2013, 117, 8619−8627

Scheme 3. Schematic Energy Diagram of Operation Principle of the DSSCs with ZnO HSN Photoanode and Graphene/ZnO HSN Photoanode, Respectively, Illustrating the Electron Injection from Excited Dye into ZnO and Transport of the Injected Electrons to the Collection Electrode

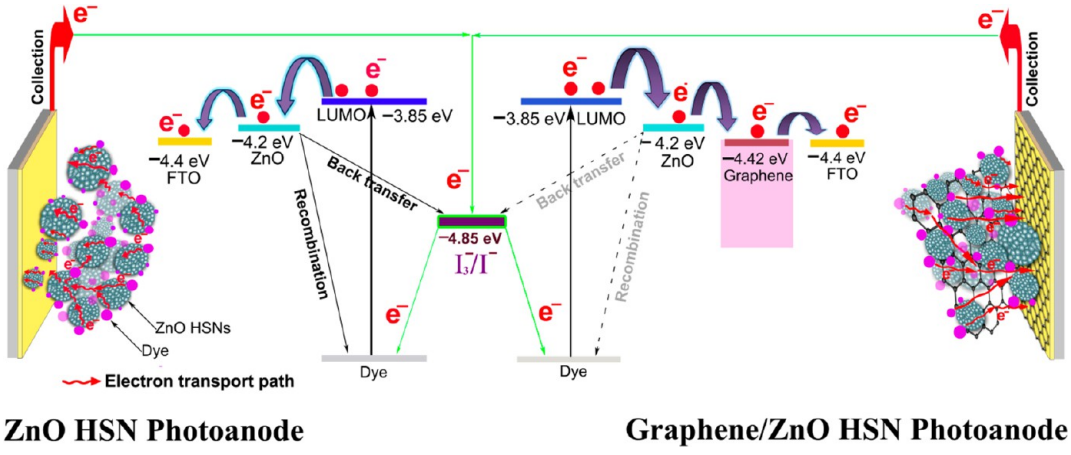

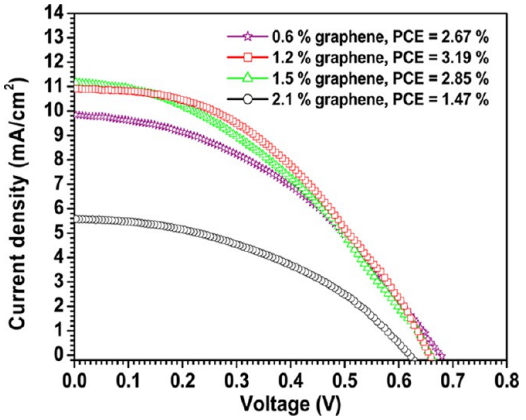

Figure 8. Current−voltage (J−V) characteristics of the DSSCs constructed using the graphene/ZnO HSN composite photoanode (3 μm thick) with different graphene loading contents (0.6 wt %, 1.2 wt %, 2.1 wt %, and 4.0 wt %, respectively) under a simulated illumination with a light intensity of 100 mW/cm^2 (AM 1.5).

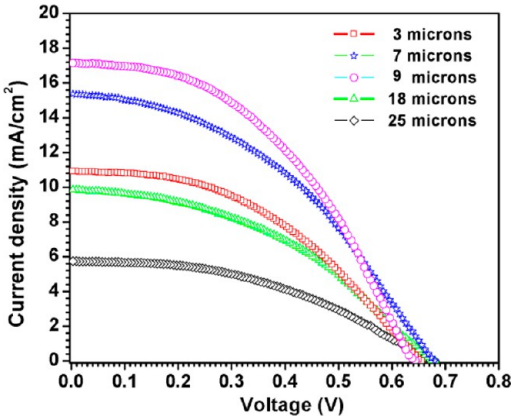

Figure 9. (a) Current−voltage (J−V) characteristics of the DSSCs constructed using the graphene/ZnO HSN composite photoanode (1.2 wt % graphene loading) with different thickness (3 μm, 7 μm, 9 μm, 18 μm, and 25 μm, respectively) under a simulated illumination with a light intensity of 100 mW/cm^2 (AM 1.5).

Table 3. Photovoltaic Parameters of the DSSCs Based on the Graphene/ZnO HSN Composite Photoanodes with Different Graphene Loading Contents

graphene/ZnO HSN composite photoanode	thickness (μm)	V_{oc} (V)	J_{sc} (mA/cm^2)	FF (%)	PCE (%)
0.6 wt % graphene loading	3	0.69	9.80	45.20	2.67
1.2 wt % graphene loading	3	0.66	10.89	47.60	3.19
1.5 wt % graphene loading	3	0.68	11.09	38.44	2.85
2.1 wt % graphene loading	3	0.64	5.55	39.16	1.47
4.0 wt % graphene loading	3	N/A	N/A	N/A	N/A

Table 4. Photovoltaic Parameters of the DSSCs Based on the Graphene/ZnO HSN Composite Photoanodes with Different Photoanode Thickness

graphene/ZnO HSN composite photoanode	thickness (μm)	V_{oc} (V)	J_{sc} (mA/cm^2)	FF (%)	PCE (%)
1.2 wt % graphene loading	3	0.66	10.89	47.60	3.19
1.2 wt % graphene loading	7	0.68	15.32	41.15	5.07
1.2 wt % graphene loading	9	0.67	17.11	42.03	5.86
1.2 wt % graphene loading	18	0.69	9.80	38.83	2.77
1.2 wt % graphene loading	25	0.69	5.72	36.21	1.58

have not counteracted the huge electron recombination loss during the electron transport to the collection electrode within the thicker photoanodes. Correspondingly, the total conversion efficiencies of the DSSCs suffering from the decreased photocurrent were inevitably decreased.

4. CONCLUSIONS

In conclusion, we reported for the first time the incorporation of graphene into the matrix of ZnO HSN photoanodes of the DSSCs for improving photogenerated electron transport. It was found that incorporating graphene effectively decreased the internal resistance within the photoanodes and prolonged the

dx.doi.org/10.1021/jp312379b | J. Phys. Chem. C 2013, 117, 8619−8627

Table 5. Comparison between Our Work and Previously Published Works

reference	photoanode	thickness (μm)	PCE (%)
Our work	Graphene/ZnO HSN	3	3.19
48	ZnO HSN	3.5	2.25
49	Iodine-doped ZnO HSN	8	4.5
Our work	Graphene/ZnO HSN	9	5.86
5	ZnO HSN	10	3.51
7	ZnO HSN	10	4.4
8	ZnO HSN	27	5.34

electron lifetime, which can reduce the electron recombination loss. Thus, the DSSCs with incorporating an optimal amount (1.2 wt %) of graphene showed the markedly enhancement in PCE compared with the DSSCs without graphene. The results demonstrate potential application of graphene for enhancing the performance of nanoparticles-based DSSCs that can be produced on a large scale by a low-cost and high-efficiency roll-to-roll process.

■ ASSOCIATED CONTENT

Ⓢ Supporting Information

Experimental section of synthesizing graphene oxide and ZnO HSNs, schematic diagram for the preparation of graphene film electrodes, and some supplementary SEM images are provided. This information is available free of charge via the Internet at http://pubs.acs.org.

■ AUTHOR INFORMATION

Corresponding Author

*Phone: +86 25 83792632. Fax: +86 25 83792939. E-mail: fxu@seu.edu.cn (F. Xu); slt@seu.edu.cn (L.-T. Sun).

Author Contributions

F. X., J. C., and X. W. contributed equally to this work.

Notes

The authors declare no competing financial interest.

■ ACKNOWLEDGMENTS

Helpful discussions with Binjie Wang and Tao Xu are appreciated. This work was supported by the National Basic Research Program of China (973 Program, Grant Nos. 2011CB707601 and 2009CB623702), the National Natural Science Foundation of China (NSFC, Grant Nos. 21243011, 61106055, 61274114, 51071044, 51202028, and 61006011), the Fundamental Research Funds for the Central Universities, China Postdoctoral Science Foundation Funded Project (Grant Nos. 20100470066 and 201104501, 2012M520053), and Jiangsu Planned Projects for Postdoctoral Research Funds (Grant No. 0902003B).

■ REFERENCES

(1) Oregan, B.; Gratzel, M. A Low-Cost, High-Efficiency Solar Cell Based on Dye-Sensitized Colloidal TiO_2 Films. *Nature* **1991**, *353*, 737−739.

(2) Saito, M.; Fujihara, S. Large Photocurrent Generation in Dye-Sensitized ZnO Solar Cells. *Energy Environ. Sci.* **2008**, *1*, 280−283.

(3) Xu, F.; Sun, L. T. Solution-Derived ZnO Nanostructures for Photoanodes of Dye-Sensitized Solar Cells. *Energy Environ. Sci.* **2011**, *4*, 818−841.

(4) Keis, K.; Bauer, C.; Boschloo, G.; Hagfeldt, A.; Westermark, K.; Rensmo, H.; Siegbahn, H. Nanostructured ZnO Electrodes for Dye-Sensitized Solar Cell Applications. *J. Photochem. Photobiol. A* **2002**, *148*, 57−64.

(5) Chou, T. P.; Zhang, Q. F.; Fryxell, G. E.; Cao, G. Z. Hierarchically Structured ZnO Film for Dye-Sensitized Solar Cells with Enhanced Energy Conversion Efficiency. *Adv. Mater.* **2007**, *19*, 2588−2592.

(6) Zhang, Q. F.; Chou, T. R.; Russo, B. S.; Jenekhe, A.; Cao, G. Z. Aggregation of ZnO Nanocrystallites for High Conversion Efficiency in Dye-Sensitized Solar Cells. *Angew. Chem., Int. Ed.* **2008**, *47*, 2402−2406.

(7) Zhang, Q. F.; Chou, T. P.; Russo, B.; Jenekhe, S. A.; Cao, G. Z. Polydisperse Aggregates of ZnO Nanocrystallites: A Method for Energy-Conversion-Efficiency Enhancement in Dye-Sensitized Solar Cells. *Adv. Funct. Mater.* **2008**, *18*, 1654−1660.

(8) Cheng, H. M.; Hsieh, W. F. High-Efficiency Metal-Free Organic-Dye-Sensitized Solar Cells with Hierarchical ZnO Photoelectrode. *Energy Environ. Sci.* **2010**, *3*, 442−447.

(9) Yoshida, T.; Zhang, J. B.; Komatsu, D.; Sawatani, S.; Minoura, H.; Pauporte, T.; Lincot, D.; Oekermann, T.; Schlettwein, D.; Tada, H.; et al. Electrodeposition of Inorganic/Organic Hybrid Thin Films. *Adv. Funct. Mater.* **2009**, *19*, 17−43.

(10) Nissfolk, J.; Fredin, K.; Hagfeldt, A.; Boschloo, G. Recombination and Transport Processes in Dye-Sensitized Solar Cells Investigated under Working Conditions. *J. Phys. Chem. B* **2006**, *110*, 17715−17718.

(11) Gratzel, M. Solar Energy Conversion by Dye-Sensitized Photovoltaic Cells. *Inorg. Chem.* **2005**, *44*, 6841−6851.

(12) Gratzel, M. Conversion of Sunlight to Electric Power by Nanocrystalline Dye-Sensitized Solar Cells. *J. Photochem. Photobiol. A* **2004**, *164*, 3−14.

(13) Law, M.; Greene, L. E.; Johnson, J. C.; Saykally, R.; Yang, P. D. Nanowire Dye-Sensitized Solar Cells. *Nat. Mater.* **2005**, *4*, 455−459.

(14) Baxter, J. B.; Walker, A. M.; Ommering, K.; Aydil, E. S. Synthesis and Characterization of ZnO Nanowires and Their Integration into Dye-Sensitized Solar Cells. *Nanotechnology* **2006**, *17*, S304−S312.

(15) Xu, C. K.; Shin, P.; Cao, L. L.; Gao, D. Preferential Growth of Long ZnO Nanowire Array and Its Application in Dye-Sensitized Solar Cells. *J. Phys. Chem. C* **2010**, *114*, 125−129.

(16) Qiu, J. J.; Li, X. M.; Zhuge, F. W.; Gan, X. Y.; Gao, X. D.; He, W. Z.; Park, S. J.; Kim, H. K.; Hwang, Y. H. Solution-Derived 40 μm Vertically Aligned ZnO Nanowire Arrays as Photoelectrodes in Dye-Sensitized Solar Cells. *Nanotechnology* **2010**, *21*, 195602.

(17) Xu, F.; Sun, L. T.; Dai, M.; Lu, Y. N. Fluorine-Ion-Mediated Electrodeposition of Rhombus-Like ZnFOH Nanorod Arrays: An Intermediate Route to Novel ZnO Nanoarchitectures. *J. Phys. Chem. C* **2010**, *114*, 15377−15382.

(18) Martinson, A. B. F.; Goes, M. S.; Fabregat-Santiago, F.; Bisquert, J.; Pellin, M. J.; Hupp, J. T. Electron Transport in Dye-Sensitized Solar Cells Based on ZnO Nanotubes: Evidence for Highly Efficient Charge Collection and Exceptionally Rapid Dynamics. *J. Phys. Chem. A* **2009**, *113*, 4015−4021.

(19) Wang, X. Y.; Tian, Z. P.; Yu, T.; Tian, H. M.; Zhang, J. Y.; Yuan, S. K.; Zhang, X. B.; Li, Z. S.; Zou, Z. G. Effective Electron Collection in Highly (110)-Oriented ZnO Porous Nanosheet Framework Photoanode. *Nanotechnology* **2010**, *21*, 065703.

(20) Lin, C. Y.; Lai, Y. H.; Chen, H. W.; Chen, J. G.; Kung, C. W.; Vittal, R.; Ho, K. C. Highly Efficient Dye-Sensitized Solar Cell with A ZnO Nanosheet-Based Photoanode. *Energy Environ. Sci.* **2011**, *4*, 3448−3455.

(21) Lin, C. F.; Lin, H.; Li, J. B.; Li, X. Electrodeposition Preparation of ZnO Nanobelt Array Films and Application to Dye-Sensitized Solar Cells. *J. Alloys Compd.* **2008**, *462*, 175−180.

(22) Yodyingyong, S.; Zhang, Q. F.; Park, K.; Dandeneau, C. S.; Zhou, X. Y.; Triampo, D.; Cao, G. Z. ZnO Nanoparticles and Nanowire Array Hybrid Photoanodes for Dye-Sensitized Solar Cells. *Appl. Phys. Lett.* **2010**, *96*, 073115.

(23) Jiang, C. Y.; Sun, X. W.; Tan, K. W.; Lo, G. Q.; Kyaw, A. K. K.; Kwong, D. L. High-Bendability Flexible Dye-Sensitized Solar Cell with

A Nanoparticle-Modified ZnO-Nanowire Electrode. *Appl. Phys. Lett.* **2008**, *92*, 143101.
(24) Xu, F.; Dai, M.; Lu, Y. N.; Sun, L. T. Hierarchical ZnO Nanowire-Nanosheet Architectures for High Power Conversion Efficiency in Dye-Sensitized Solar Cells. *J. Phys. Chem. C* **2010**, *114*, 2776−2782.
(25) Qiu, J. H.; Guo, M.; Wang, X. D. Electrodeposition of Hierarchical ZnO Nanorod-Nanosheet Structures and Their Applications in Dye-Sensitized Solar Cells. *ACS Appl. Mater. Interface* **2011**, *3*, 2358−2367.
(26) Ko, S. H.; Lee, D.; Kang, H. W.; Nam, K. H.; Yeo, J. Y.; Hong, S. J.; Grigoropoulos, C. P.; Sung, H. J. Nanoforest of Hydrothermally Grown Hierarchical ZnO Nanowires for A High Efficiency Dye-Sensitized Solar Cell. *Nano Lett.* **2011**, *11*, 666−671.
(27) Listorti, A.; Oregan, B.; Durrant, J. R. Electron Transfer Dynamics in Dye-Sensitized Solar Cells. *Chem. Mater.* **2011**, *23*, 3381−3399.
(28) Novoselov, K. S.; Geim, A. K.; Morozov, S. V.; Jiang, D.; Zhang, Y.; Dubonos, S. V.; Grigorieva, I. V.; Firsov, A. A. Electric Field Effect in Atomically Thin Carbon Films. *Science* **2004**, *306*, 666−669.
(29) Hummers, W. S.; Offeman, R. E. Preparation of Graphitic Oxide. *J. Am. Chem. Soc.* **1958**, *80*, 1339−1339.
(30) Bi, H. C.; Yin, K. B.; Xie, X.; Zhou, Y. L.; Wan, N.; Xu, F.; Banhart, F.; Sun, L. T; Ruoff, R. S. Low Temperature Casting of Graphene with High Compressive Strength. *Adv. Mater.* **2012**, *24*, 5124−5129.
(31) Jezequel, D.; Guenot, J.; Jouini, N.; Fievet, F. Preparation and Morphological Characterization of Fine, Spherical, Monodisperse Particles of ZnO. *Mater. Sci. Forum* **1994**, *152*−*153*, 339−342.
(32) Wu, Z. C.; Chen, Z. H.; Du, X.; Logan, J. M.; Sippel, J.; Nikolou, M.; Kamaras, K.; Reynolds, J. R.; Tanner, D. B.; Hebard, A. F.; et al. Transparent, Conductive Carbon Nanotube Films. *Science* **2004**, *305*, 1273−1276.
(33) Nethravathi, C.; Rajamathi, M. Chemically Modified Graphene Sheets Produced by The Solvothermal Reduction of Colloidal Dispersions of Graphite Oxide. *Carbon* **2008**, *46*, 1994−1998.
(34) Li, D.; Muller, M. B.; Gilje, S.; Kaner, R. B.; Wallace, G. G. Processable Aqueous Dispersions of Graphene Nanosheets. *Nat. Nanotechnol.* **2008**, *3*, 101−105.
(35) Li, X. L.; Zhang, G. Y.; Bai, X. D.; Sun, X. M.; Wang, X. R.; Wang, E. G.; Dai, H. J. Highly Conducting Graphene Sheets and Langmuir-Blodgett Films. *Nat. Nanotechnol.* **2008**, *3*, 538−542.
(36) Zhang, J. L.; Yang, H. J.; Shen, G. X.; Cheng, P.; Zhang, J. Y.; Guo, S. W. Reduction of Graphene Oxide Vial-Ascorbic Acid. *Chem. Commun.* **2010**, *46*, 1112−1114.
(37) Yang, N. L.; Zhai, J.; Wang, D.; Chen, Y. S.; Jiang, L. Two-Dimensional Graphene Bridges Enhanced Photoinduced Charge Transport in Dye-Sensitized Solar Cells. *ACS Nano* **2010**, *4*, 887−894.
(38) Sun, S. R.; Gao, L.; Liu, Y. Q. Enhanced Dye-Sensitized Solar Cell Using Graphene-TiO_2 Photoanode Prepared by Heterogeneous Coagulation. *Appl. Phys. Lett.* **2010**, *96*, 083113.
(39) Brown, P.; Takechi, K.; Kamat, P. V. Electrophoretic Deposition of CdSe-C_{60} Composite Films and Capture of Photogenerated Electrons with nC_{60} Cluster Shell. *J. Phys. Chem. C* **2008**, *112*, 4776−4782.
(40) Kongkanand, A.; Dominguez, R. M.; Kamat, P. V. Single Wall Carbon Nanotube Scaffolds for Photoelectrochemical Solar Cells. Capture and Transport of Photogenerated Electrons. *Nano Lett.* **2007**, *7*, 676−680.
(41) Chen, J.; Li, C.; Zhao, D. W.; Lei, W.; Zhang, Y.; Cole, M. T.; Chu, D. P.; Wang, B. P.; Cui, Y. P.; Sun, X. W.; Milne, W. I. A Quantum Dot Sensitized Solar Cell Based on Vertically Aligned Carbon Nanotube Templated ZnO Arrays. *Electrochem. Commun.* **2010**, *12*, 1432−1435.
(42) Kern, R.; Sastrawan, R.; Ferber, J.; Stangl, R.; Luther, J. Modeling and Interpretation of Electrical Impedance Spectra of Dye Solar Cells Operated under Open-Circuit Conditions. *Electrochim. Acta* **2002**, *47*, 4213−4225.
(43) Wang, M. K.; Chen, P.; Humphry-Baker, R.; Zakeeruddin, S. M.; Gratzel, M. The Influence of Charge Transport and Recombination on The Performance of Dye-Sensitized Solar Cells. *ChemPhysChem* **2009**, *10*, 290−299.
(44) Bisquert, J. Chemical Capacitance of Nanostructured Semiconductors: Its Origin and Significance for Nanocomposite Solar Cells. *Phys. Chem. Chem. Phys.* **2003**, *5*, 5360−5364.
(45) Choi, H. B.; Kang, S. O.; Ko, J.; Gao, G. H.; Kang, H. S.; Kang, M. S.; Nazeeruddin, M. K.; Gratzel, M. An Efficient Dye-Sensitized Solar Cell with An Organic Sensitizer Encapsulated in A Cyclodextrin Cavity. *Angew. Chem., Int. Ed.* **2009**, *48*, 5938−5941.
(46) Song, J. L.; Yin, Z. Y.; Yang, Z. J.; Amaladass, P.; Wu, S. X.; Ye, J.; Zhao, Y.; Deng, W. Q.; Zhang, H.; Liu, X. W. Enhancement of Photogenerated Electron Transport in Dye-Sensitized Solar Cells with Introduction of A Reduced Graphene Oxide-TiO_2 Junction. *Chem.—Eur. J.* **2011**, *17*, 10832−10837.
(47) Wang, X.; Zhi, L. J.; Mullen, K. Transparent, Conductive Graphene Electrodes for Dye-Sensitized Solar Cells. *Nano Lett.* **2008**, *8*, 323−327.
(48) Zhang, Y. Z.; Wu, L. H.; Liu, Y. P.; Xie, E. Q. Improvements to The Hierarchically Structured ZnO Nanosphere Based Dye-Sensitized Solar Cells. *J. Phys. D: Appl. Phys.* **2009**, *42*, 085105.
(49) Zheng, Y. Z.; Tao, X.; Hou, Q.; Wang, D. T.; Zhou, W. L.; Chen, J. F. Iodine-Doped ZnO Nanocrystalline Aggregates for Improved Dye-Sensitized Solar Cells. *Chem. Mater.* **2011**, *23*, 3−5.